JOURNAL OF NEUROTRAUMA 28:775–785 (May 2011)

DOI: 10.1089/neu.2010.1692

High Intracranial Pressure Effects on Cerebral Cortical Microvascular Flow in Rats

Denis E. Bragin, Rachel C. Bush, Wolfgang S. Müller, and Edwin M. Nemoto

Abstract

To manage patients with high intracranial pressure (ICP), clinicians need to know the critical cerebral perfusion pressure (CPP) required to maintain cerebral blood flow (CBF). Historically, the critical CPP obtained by decreasing mean arterial pressure (MAP) to lower CPP was 60 mm Hg, which fell to 30 mm Hg when CPP was reduced by increasing ICP. We examined whether this decrease in critical CPP was due to a pathological shift from capillary (CAP) to high-velocity microvessel flow or thoroughfare channel (TFC) shunt flow. Cortical microvessel red blood cell velocity and NADH fluorescence were measured by *in vivo* two-photon laser scanning microscopy in rats at CPP of 70, 50, and 30 mm Hg by increasing ICP or decreasing MAP. Water content was measured by wet/dry weight, and cortical perfusion by laser Doppler flux. Reduction of CPP by raising ICP increased TFC shunt flow from 30.4 ± 2.3% to 51.2 ± 5.2% (mean ± SEM, $p < 0.001$), NADH increased by 20.3 ± 6.8% and 58.1 ± 8.2% ($p < 0.01$), and brain water content from 72.9 ± 0.47% to 77.8 ± 2.42% ($p < 0.01$). Decreasing CPP by MAP decreased TFC shunt flow with a smaller rise in NADH and no edema. Doppler flux decreased less with increasing ICP than decreasing MAP. The decrease seen in the critical CPP with increased ICP is likely due to a redistribution of microvascular flow from capillary to microvascular shunt flow or TFC shunt flow, resulting in a pathologically elevated CBF associated with tissue hypoxia and brain edema, characteristic of non-nutritive shunt flow.

Key words: brain edema; cerebrovascular shunts; intracranial hypertension; NADH; thoroughfare channels

Introduction

Increased intracranial pressure (ICP) is a serious consequence of brain edema after a variety of cerebral insults such as ischemic or traumatic brain injury, which may threaten perfusion to the entire brain. To ensure maintenance of adequate cerebral perfusion in the face of increased ICP, clinicians need to know the critical cerebral perfusion pressure (CPP) marking the lower limit of cerebral blood flow (CBF) autoregulation. Historically, this question was addressed in animal studies in which the critical CPP for CBF autoregulation was defined by decreasing mean arterial pressure (MAP), resulting in a critical CPP of 60 to 70 mm Hg (Barry et al., 1982; Ingvar and Lasssen, 1977; Mathew et al., 1975; Rosner et al., 1995). However, clinically, CPP often decreases secondary to an increase in ICP rather than a decrease in MAP, which raises the question of whether the critical CPP threshold for CBF autoregulation is the same when CPP is reduced by increasing ICP as opposed to decreasing MAP.

Recognizing that CBF autoregulation may differ depending on whether CPP changes are due to increased ICP or decreased MAP, comparative studies were done in dogs (Miller et al., 1972), nonhuman primates (Grubb et al., 1975; Johnston et al., 1972), and rats (Hauerberg and Juhler, 1994). The critical CPP for CBF autoregulation was 30 mm Hg when CPP was decreased by increasing ICP, compared to 60 mm Hg by decreasing MAP (Grubb et al., 1975; Miller et al., 1972), suggesting that CBF autoregulation is better preserved when CPP is reduced by increasing ICP. However, we hypothesized that the reduction in critical CPP to 30 mm Hg obtained when CPP is reduced by increasing ICP is due to pathological shunt flow, and speculate that this microvessel shunt flow is the previously described thoroughfare channels (TFC) maintaining an apparent CBF.

The existence of cerebrovascular shunts has been largely denied or ignored among investigators of the cerebrovascular circulation, despite substantial evidence for their existence. Histological studies have shown the presence of TFC shunts in the human brain, primarily at the top and bottom cortical layers and through the subcortical and periventricular white matter (Hasegawa et al., 1967; Motti et al., 1986; Ravens, 1974). Cerebrovascular shunts are also suggested by reports of "red

Department of Neurosurgery, University of New Mexico, Albuquerque, New Mexico.

veins" in infarcted or contused brain (Feindel and Perot, 1965; Feindel et al., 1971). Shunt flow peaks are also suggested in radioactive CBF measurements (Haggendal et al., 1965; Lassen and Perl, 1979). Perhaps the most convincing evidence of shunt flow within the brain is the observation of two populations of microvessel flow distinguished by flow velocities above and below 1.0 mm/sec (Hudetz et al., 1995, 1996, 1997, 1997a). Microvessels with flow velocities >1.0 mm/sec showed no autoregulation, whereas microvessels with flow velocities <1.0 mm/sec showed perfect autoregulation. Although the percentage of high-velocity relative to low-velocity microvessels in the normal rat brain is unknown, it is believed to represent a small percentage of the total number of microvessels. However, how small this distribution is has not been quantitatively determined or even estimated. Rarefaction of brain capillaries in infarcted brain with large-diameter microvessels (Tomita, 1968) documented by hyperemia through these vessels also supports the existence of cerebrovascular shunts (Ginsberg et al., 1987; Hughes et al., 1989; Ito et al., 2000). Our aim in this study was to determine by *in vivo* two-photon laser scanning microscopy (2PLSM), changes in microvascular capillary (CAP) flow when the critical CPP is defined by increasing ICP as opposed to decreasing MAP.

Methods

Animals and surgical procedures

All procedures were approved by the Institutional Animal Care and Use Committee at the University of New Mexico Health Sciences Center under protocol #100916, performed in accordance with the National Institutes of Health (NIH) Guide for the Care and Use of Laboratory Animals. Male Sprague-Dawley (SD) rats ($n = 45$) weighing between 300 and 350 g were obtained from Harlan Laboratories (Indianapolis, IN) and acclimated for 1 week before use. The rats were anesthetized in a box insufflated with 4% isoflurane/50% nitrous oxide and 50% oxygen, intubated with a 14 g × 1.9" catheter, and mechanically ventilated (Model 683; Harvard Apparatus, Holliston, MA) on 2% isoflurane/30% oxygen/70% nitrous oxide, at a tidal volume of 2.0–2.5 mL and a respiratory rate of 55–65/min. The animals were placed on a heating pad to maintain rectal temperature at 37 ± 0.5°C, and injected with atropine (0.2 mg IP) to decrease oral and pulmonary secretions. Femoral artery catheters (PE-50) were inserted to monitor arterial blood pressure and for arterial blood samples (0.3 mL each) for blood gas analyses. Femoral vein catheters (PE-50) were inserted for fluid replacement (lactated Ringer's solution, 2 mL/2 h), fluorescein dextran dye injection, and MAP manipulations by blood withdrawal. After that, the rats were placed in a sterotaxic head holder for cranial surgery.

A catheter (PE-50) was inserted through the atlanto-occipital membrane into the cisterna magna and glued (cyanoacrylate glue) in place for ICP monitoring and to manipulate ICP by adjusting the height of a reservoir of artificial cerebrospinal fluid (ACSF). For imaging, a craniotomy (5-mm diameter) was made over the left parietal cortex 1 mm lateral to the sagittal suture and 1 mm anterior to the lambdoidal suture without traumatizing the brain or dura. The craniotomy was filled with 2% agarose gel in saline and a cover glass was placed over the craniotomy and glued onto the skull (cyanoacrylate glue). A cranial thermistor (1-mm diameter) temperature probe was inserted 5 mm into the temporal muscle adjacent to the skull to estimate brain temperature.

Experimental paradigm

The animals were studied in three groups of 10 rats each (Table 1): (1) a control group, (2) a CPP-ICP group for ICP manipulation of CPP, and (3) a CPP-MAP group for MAP manipulation of CPP. In the CPP-MAP group, arterial blood pressure and thereby CPP was reduced by progressive withdrawal of venous blood into a syringe with heparinized saline. The total amount of blood withdrawn ranged from 3–5 mL. In the CPP-ICP group, the increase in ICP resulted in a Cushing reflex (i.e., a sympathetic discharge and rise in arterial pressure that was countered by withdrawal of blood via the venous catheter while continuously monitoring arterial pressure to regulate CPP). The time spent at each level was 30 min, which was sufficient time for stabilization of physiological variables and to make microvascular and physiological measurements. Measured variables were: microvascular red blood cell (RBC) flow velocity, reduced nicotinamide adenine dinucleotide (NADH) fluorescence as an indicator of tissue oxygenation, cortical Doppler flux, and cortical water content. Rectal and temporal muscle temperatures and arterial and intracranial pressures were continuously monitored. Arterial blood gases, oxygen content, pH, glucose, and electrolytes were measured at each CPP level by an iSTAT point-of-care device with a CG8+ cartridge (ABAXIS, Union City, CA). Arterial pressure, ICP, and CBF were continuously recorded on a laptop computer using Biopac preamplifiers and software (Goleta, CA).

Cortical doppler flux

Relative changes in cortical perfusion were measured by Doppler flux in the vicinity of the 2PLSM measurements using a single-fiber 0.8-mm-diameter surface Doppler probe (DRT4; Moor Instruments, Axminster, U.K.) secured laterally on the temporal bone through a small non-penetrating thinned skull burr hole. Continuous measurements were made throughout

Table 1. Experimental Paradigm for the Three Study Groups

Control group			*ICP-CPP group*			*MAP-CPP group*		
CPP	*MAP*	*ICP*	*CPP*	*MAP*	*ICP*	*CCP*	*MAP*	*ICP*
70	80	10	70	80	10	70	80	10
70	80	10	50	80	30	50	60	10
70	80	10	30	80	50	30	40	10

$n = 10$ rats per group, all measurements in mm Hg.
CPP, cerebral perfusion pressure; MAP, mean arterial pressure; ICP, intracranial pressure.

the study by noting the changes in Doppler flux with changes in CPP and allowing equilibration of Doppler flux at each CPP level.

In vivo *two-photon laser scanning microscopy of RBC flow velocity*

After surgery, the rats were moved to the 2PLSM microscope platform for imaging studies. Body temperature was maintained at 37 ± 0.5°C with a water heating pad. Arterial blood samples (0.3 mL each) were drawn at each CPP level for arterial blood gas, oxygen content, pH, and electrolyte analysis.

Fluorescein isothiocyanate-labeled dextran (20-kDa) in physiological saline (5% wt/vol) was injected at an initial serum dye concentration of 150 μM (Kleinfeld et al., 1998). Fluorescent serum was visualized using an Olympus BX 51WI upright microscope and water-immersion LUMPlan FL/IR 20×/0.50 W objective. Excitation was provided by a Prairie View Ultima multiphoton microscopy laser scan unit powered by a Millennia VI 6 W diode laser source pumping a Tsunami Ti:sapphire laser (Spectra-Physics, Mountain View, CA) tuned to 810-nm center wavelength. Band-pass-filtered epifluorescence (560–660 nm) was collected by the photomultiplier tubes of the Prairie View Ultima system. Images (512×512 pixels, 0.15 μm/pixel in the x- and y-axes) or line scans were acquired using Prairie View software. A total average power of 30–300 mW was delivered to the cortex, the higher values to image at greater depths, always using the lowest intensity required for adequate signal-to-noise ratio.

In offline analyses using NIH ImageJ software, three-dimensional anatomy of the vasculature in regions of interest were reconstructed from two-dimensional (planar) scans of the fluorescence intensity obtained at successive focal depths in the cortex (XYZ stack). Attenuation of the signal along the Z-direction was corrected by multiplication of each XY image by factors determined empirically from plots of the intensity variation of background fluorescence as a function of depth. RBC motion was determined from line-scan measurements (i.e., repetitive scans of the laser along the central axis of a microvessel at several depths [100–300 μm] from the pia mater) (Kleinfeld et al., 1998). We oriented the direction of the scan, and on average scanned a distance of 35 μm with a spatial resolution of 0.7 μm per pixel, a temporal resolution of 2 msec per scan, and a record length of 128 sec.

Microvessel selection and identification

The selection of capillary microvessels was based on tortuosity, degree of branching, and diameters ranging from 3–8 μm (Hauck et al., 2004; Hudetz et al., 2000; Motti et al., 1986; Seylaz et al., 1999). Multiple records were taken from the same vessel and mean microvessel RBC velocity and standard error of the mean (SEM) were determined. A total of approximately 100 microvessels were scanned at each CPP, and the diameter of each scanned vessel was measured.

In vivo *two-photon laser imaging of NADH*

NADH autofluorescence was measured using 2PLSM as described above. Twenty planar scans of the NADH fluorescence intensity were obtained with 10-μm steps starting 100 μm deep from the pia matter for each CPP level. Fluorescence was emitted by 740-nm center wavelength and bandpass filtered at 425–475 nm (Takano et al., 2007). In offline analyses using NIH ImageJ software, average intensities were calculated from the maximal intensity projection image for each CPP.

Parietal cortex water content

In separate studies, parietal cortex tissue (20–100 mg) was rapidly sampled through the craniotomy at each CPP. The tissue specimens were immediately weighed on pre-weighed, pre-dried aluminum foil weighing boats to obtain the wet weight on a scale with a sensitivity of ± 0.1 mg. Dry weight was determined after drying the tissue for 48 h in a drying oven set at 110°C. Cortical water content was calculated as (wet weight – dry weight)/wet weight × 100. Comparisons in 10 rats were made between the method of sampling cortical tissue through the craniotomy and decapitation of the rat, removal of the brain from the skull, and taking of a piece of the cortex for measurement of water content.

Statistical analysis

Statistical analyses were done by independent Student's *t*-test or the Kolgomorov-Smirnov test where appropriate. Significance was set at $p < 0.05$. Data are presented as mean ± SEM.

Results

Arterial blood gases, oxygen content, glucose, pH and electrolytes, and rectal and cranial temperatures were monitored and maintained within normal limits throughout the study for each group with no significant differences between groups (Table 2). Blood glucose levels were significantly elevated early after surgical preparation, likely due to the stress of surgery and anesthesia, with no significant differences between groups. Variations in blood gases were adjusted by manipulation of the rate and volume of the ventilator. Base deficits below −5.0 mEq/L were corrected by slow IV injection of 8.4% sodium bicarbonate calculated as 0.5 × 0.3 body weight in kilograms × base deficit in mEq/mL = mEq $NaHCO_3$.

RBC flow velocities by 2PLSM

Line scans (Fig. 1b) were performed at each CPP on approximately 100 microvessels (3–15 μm in diameter) from the regions imaged by 2PLSM microscopy at several depths (100–300 μm) from the pia mater (Fig. 1a). Figure 1c illustrates line scan data from two microvessels where the tracks of nonfluorescent RBCs are represented as dark stripes and labeled plasma as bright stripes. The slope of the stripes inversely reflects RBC velocity, showing that flow velocity was slower in the first than in the second microvessel.

The panels in Figure 1d and 1e show the normalized frequency distribution of flow velocities in the control group at a CPP of 70 mm Hg and at a CPP of 50 and 30 mm Hg by increasing ICP (1d) or decreasing MAP (1e). At the control CPP of 70 mm Hg, there was no difference in the distribution of flow velocities between the ICP and MAP groups. RBC speeds at normal CPP (70 mm Hg) varied from 0.14 to 4.19 mm/sec (left panels in Fig. 1d and e). At the control CPP of 70 mm Hg, the proportion of microvessels with velocities < 1 mm/sec was 67.2 ± 5.75%, and was significantly more than microvessels

Table 2. Temperature, Arterial Blood Gas, and Electrolyte Values in the Three Study Groups

Groups	*Control*		*ICP-CPP*		*MAP-CPP*	
Variable	*Mean*	*SEM*	*Mean*	*SEM*	*Mean*	*SEM*
Rectal temperature (°C)	37.2	1.1	37.4	1.2	36.9	1.5
Cranial temperature (°C)	35.6	1.5	35.4	1.3	35.8	1.6
Glucose (mg/dL)	246.5	20.5	254	31.23	230.33	54.57
Na (mM/L)	135.6	0.68	136.75	2.14	137.67	0.88
K (mM/L)	5.54	0.22	5.2	0.29	5.03	0.98
Total CO_2 (mM/L)	22.17	0.87	19.75	2.14	21	5.69
iCa (mM/L)	1.39	0.04	1.31	0.03	1.31	0.068
Hematocrit (% PCV)	41.8	0.86	39	3.11	42.33	0.88
Hemoglobin (g/dL)	13.25	1.05	13.25	1.05	14.4	0.32
pH	7.39	0.015	7.39	0.048	7.21	0.03
PCO_2 (mm Hg)	37.39	2.27	39.3	2.53	48.6	12.31
PO_2 (mm Hg)	121	17.62	116.75	14.69	121	17.62
HCO_3 (mM/L)	21.97	2.77	18.95	2.14	19.7	5.37
BEecf (mM/L)	−3.57	0.81	−4.43	2.94	−4.33	5.89
Oxygen saturation (%)	99	0.29	99.1	0.25	98.7	0. 27

Data presented as a mean ± SEM of three blood samples per animal taken at CPP of 70, 50, and 30 mm Hg or at the appropriate time points in the control group ($n = 10$ rats per group).

ICP, intracranial pressure; MAP, mean arterial pressure; CPP, cerebral perfusion pressure; SEM, standard error of the mean; PCO_2, partial arterial carbon dioxide pressure; PO^2, partial arterial oxygen pressure; PCV, packed cell volume; iCa, ionized calcium; BEecf, base excess in extracellular fluid.

with velocities >1 mm/sec, which was 32.8 ± 3.3% (left panel in Fig. 1f).

Stepwise reduction of CPP from 70 to 50 and 30 mm Hg by increasing ICP (Fig. 1d) resulted in a progressive increase in the number of microvessels with flow velocities >1.0 mm/sec, suggesting a shift of flow from capillaries to high-velocity microvessel shunts (Table 3, $p < 0.001$ compared to the MAP group). RBC speeds in the ICP group ranged from 0.069 to 8.67 mm/sec (middle and right panels in Fig. 1d). At a CPP of 50 mm Hg, the percentage distributions of low (<1 mm/sec) and high (>1 mm/sec) flow velocities were 58.4 ± 4.6% and 41.6 ± 3.4%, respectively (Table 3). Reduction of CPP to 30 mm Hg by increasing ICP caused a further increase in the percentage distribution of high (51.2 ± 5.1%) versus low (48.8 ± 4.7%) flow velocities, respectively (Table 3).

The middle panel of Figure 1f shows redistribution of RBC flow velocities with a CPP decrease to 30 mm Hg by increasing ICP. The increase in the number of microvessels with speed >1.0 mm/sec and larger diameters represents flow in the TFC (8–15 μm diameter), while microvessels with speed <1.0 mm/sec and 3–6 μm diameter represent capillary flow. An apparent decrease in flow velocity in capillaries (3–8 μm diameter), and a marked increase in flow velocity in microvessels 8–15 μm was observed at a CPP of 30 mm Hg by increasing ICP (middle panel in Fig. 1f).

In contrast to the pattern of redistribution of flow in microvessels observed in the ICP group, decreasing CPP from 70 to 50 and 30 mm Hg by reducing MAP resulted in a reduction in flow velocity at a lower CPP, without an increase in higher flow velocity microvessels or TFC shunts (Table 3, $p < 0.001$ compared to the ICP group). RBC velocities in the MAP group varied from 0.048 to 2.65 mm/sec (middle and right panels in Fig. 1e). The distribution between low and high flow velocities at a CPP of 50 mm Hg was similar to that observed at the normal CPP (70.7 ± 6.4% and 29.3 ± 4.5%, respectively; Table 3). There was a further redistribution of the percentage of low flow velocity microvessels at 30 mm Hg, of 86.1 ± 6.9% versus 13.9 ± 2.6% (Table 3 and right panel in Fig. 1f), indicating an overall reduction in capillary flow velocities at low CPP by decreasing MAP.

Laser Doppler flux

The decrease in Doppler flux with reduction of CPP by increasing ICP was significantly less than that observed by decreasing MAP (Fig. 2a). In the ICP group, Doppler flux fell to 86.7 ± 4.7% and 76.6 ± 4.5% of normal at CPP of 50 and 30 mm Hg, respectively (Fig. 2a, mean ± SEM, $p < 0.05$ and $p < 0.01$ at CPP 50 and 30 mm Hg, respectively). Doppler flux in the MAP group decreased to 72.3 ± 5.1% and 51.1 ± 5.2% from control levels at CPP of 50 and 30 mm Hg, respectively (Fig. 2a, mean ± SEM, $p < 0.01$ and $p < 0.001$ at CPP of 50 and 30 mm Hg, respectively). These results were expected from the higher CBF velocity in the ICP group compared to the decrease in the MAP group, supporting the shunting hypothesis at reduced CPP and increased ICP.

Tissue NADH

The oxidation of NADH is a sensitive indicator of the status of mitochondrial oxidation. NADH is fluorescent, whereas oxidized NAD^+ is not. Therefore optical imaging of NADH autofluorescence is a sensitive indicator of cellular oxidation and tissue oxidation state (Chance et al., 1962; Takano et al., 2007), and is used as a method to detect tissue hypoxia.

At a CPP of 70 mm Hg NADH fluorescence was evenly distributed in rat parietal cortex (Fig. 2c). Reduction of CPP by ICP elevation resulted in a marked increase in NADH fluorescence, by 20.3 ± 6.8% and 58.1 ± 8.2% from baseline CPP to 50 and 30 mm Hg, respectively (Fig. 2b and d, mean ± SEM, $^*p < 0.05$ and $^{**}p < 0.01$). Reduction of CPP by decreasing MAP also led to an increase in NADH, but it was less marked compared to the ICP group. In the MAP group, NADH increased by 11.7 ± 5.9% and 17.3 ± 7.5% from baseline at CPP of

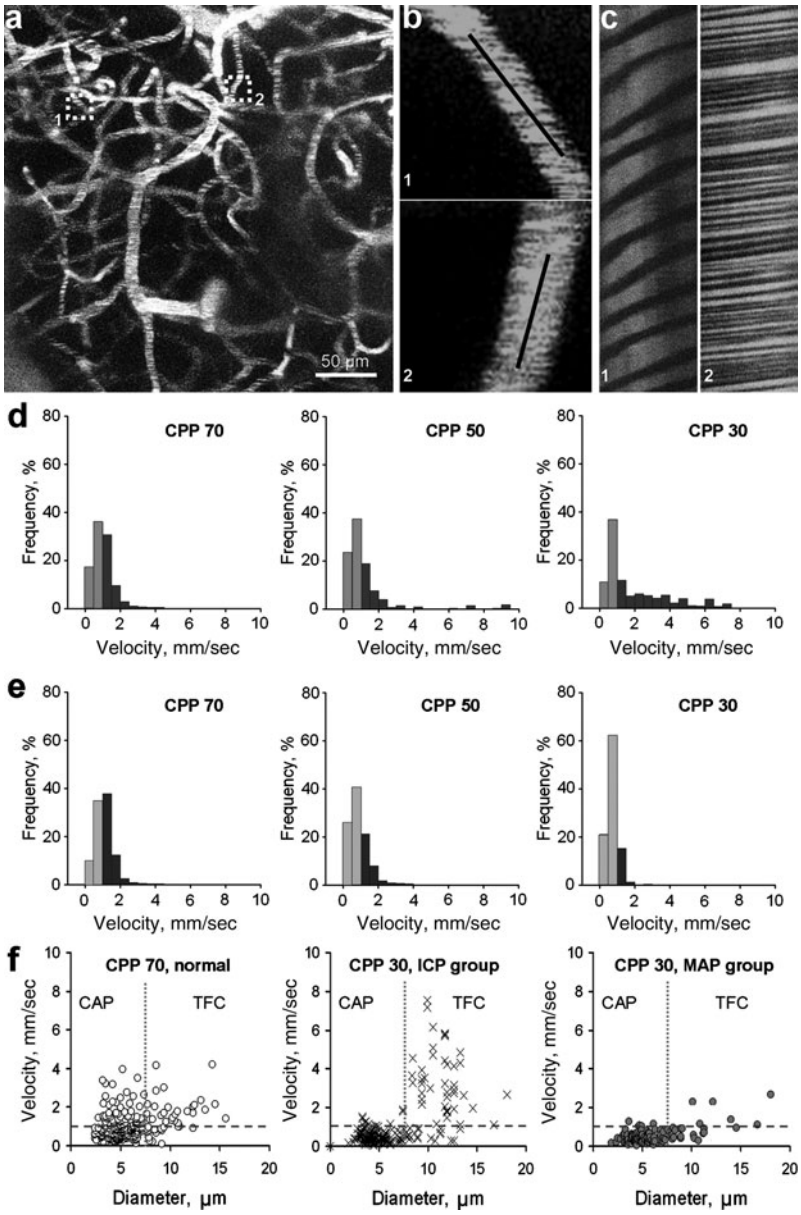

FIG. 1. Red blood cell (RBC) flow velocity changes were different during reduction of cerebral perfusion pressure (CPP) by intracranial pressure (ICP) increase versus mean arterial pressure (MAP) decrease. (**a**) Z-projection showing a region from which microvascular flow was recorded (maximal intensity projection from 20 planar scans acquired every 10 μm). (**b**) Illustration of RBC flow in microvessels shown in **a** (boxed) at higher magnification. Black lines along the microvessels represent the tracks of line scans. (**c**) Line-scan data for blood flow velocities in the two microvessels shown in **a** and **b** indicating lower flow velocity in the first microvessel than in the second. (**d**) Normalized frequency histograms showing the shift in flow velocities from below (orange-brown) to above 1.0 mm/sec (dark brown) with decreasing CPP by increasing ICP on microvessel flow velocities ($n = 10$). Progressive decreases of CPP from 70 to 50 and 30 mm Hg by increasing ICP resulted in a progressive shift to higher flow velocities, suggesting a shift from capillaries to higher flow velocity and larger thoroughfare channel TFC shunts. (**e**) Normalized frequency histograms of the effect of decreasing CPP by MAP reductions in microvessel flow velocity distribution above (light blue) and below (dark blue) 1.0 mm/sec ($n = 10$ rats/group). Decreasing CPP from 70 to 50 and 30 mm Hg by MAP reduction reduced flow velocity at a lower CPP without an increase toward higher flow velocities. Instead, the proportion of microvessels below 1.0 mm/sec increased as CPP was reduced to 50 and 30 mm Hg. (**f**) Scatterplots of RBC flow velocity versus microvessel diameter at control CPP of 70 mm Hg and CPP of 30 mm Hg by increased ICP (middle panel) and reduced MAP (right panel). The left panel shows the distribution of RBC flow velocity versus vessel diameter in rat parietal cortex microvessels (3–15 μm diameter) at normal CPP (70 mm Hg, $n = 10$ rats/group; CAP, capillaries; TFC, thoroughfare channels). The blue dashed horizontal lines demarcate a velocity of 1.0 mm/sec. The red vertical dotted lines demarcate a vessel diameter of 7 μm. The middle panel shows that the decrease of CPP to 30 mm Hg by increasing ICP caused redistribution of RBC flow velocity to higher velocities (> 1.0 mm/sec) and larger diameters (8–15 μm). Velocity in CAP (3–6 m diameter) decreased, while flow velocities in larger microvessels may indicate increases caused by TFC shunts (8–15 μm diameter; $n = 10$ rats/group). The right panel shows that the decrease of MAP to reduce CPP to 30 mm Hg decreased flow velocity in all microvessel diameters in the rat parietal cortex.

Table 3. Percentage Distribution (Mean ± SEM) of Low Capillary (CAP; <1 mm/sec) and High Thoroughfare Channel (TFC; >1 mm/sec) Flow Velocities in the Cerebral Cortex of Rats

		ICP group (%) n = *10*			*MAP group (%)* n = *10*		
CPP (mm Hg)	*MAP (mm Hg)*	*<1 mm/sec (CAP)*	*>1 mm/sec (TFC)*	*MAP (mm Hg)*	*<1 mm/sec (CAP)*	*>1 mm/sec (TFC)*	p <
70	81.3 ± 3.8	69.6 ± 5.4	30.4 ± 2.3	83.4 ± 4.1	64.8 ± 6.1	35.2 ± 4.3	0.145
50	79.6 ± 4.0	58.4 ± 4.6	41.6 ± 3.4	64.1 ± 3.2	70.7 ± 6.4	29.3 ± 4.5	0.001
30	80.5 ± 3.6	48.8 ± 4.7	51.2 ± 5.1	41.3 ± 3.4	86.1 ± 6.9	13.9 ± 2.6	0.001

p Values refer to CAP and TFC percentage comparisons of the entire distribution between the ICP and MAP groups at each CPP.
ICP, intracranial pressure; MAP, mean arterial pressure; CPP, cerebral perfusion pressure.

50 and 30 mm Hg, respectively (Fig. 2b, mean ± SEM, $p = 0.063$ and $p < 0.05$ for CPP 50 and 30 mm Hg, respectively).

Blood–brain barrier permeability

Blood–brain barrier permeability was assessed by the extravasation of fluorescein isothiocyanate-labeled dextran into the tissue (Fig. 3). The table in Figure 3 shows the number of rats out of 10 for each group that showed dye extravasation with decreasing CPP by ICP and MAP. At a CPP of 30 mm Hg by high ICP, 8/10 rats showed dye extravasation, compared to 2/10 in the MAP group. Averaged dye concentration as expressed in absolute units (a.u.) for all 10 rats in each group showed a significant increase ($p < 0.05$) at a CPP of 30 mm Hg

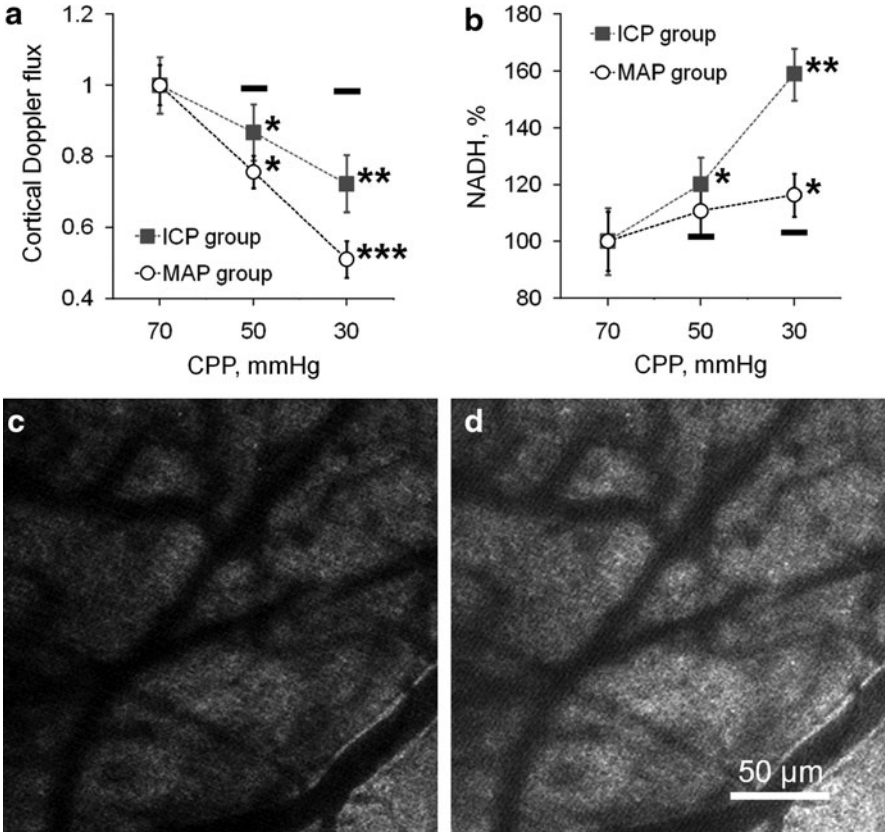

FIG. 2. Graphic illustration of changes in cortical Doppler flux and tissue hypoxia by reduced nicotinamide adenine dinucleotide (NADH) autofluorescence with changes in cerebral perfusion pressure (CPP) by increased intracranial pressure (ICP) and decreased mean arterial pressure (MAP). (**a**) The decrease in hemispheric Doppler flux when CPP was gradually reduced from 70 to 50 and 30 mm Hg by increasing ICP was less than that seen by decreasing MAP (mean ± standard error of the mean [SEM], $n = 10$ rats/group, $^*p < 0.05$, $^{**}p < 0.01$, $^{***}p < 0.001$). The dashes above the 50 and 30 mm Hg data show the Doppler flux values from the control group at normal CPP at the appropriate time points. Data were normalized to initial control levels at normal CPP (70 mm Hg). (**b**) Graph showing progression of more severe tissue hypoxia (by change of NADH autofluorescence) during reduction in CPP from 70 to 50 and 30 mm Hg by increasing ICP than by decreasing MAP. The black dashes below the 50 and 30 mm Hg data points demarcate the control NADH levels (mean ± SEM, $^*p < 0.05$, $^{**}p < 0.01$). Data were normalized to initial control levels at normal CPP (70 mm Hg). (**c**) Micrograph of baseline NADH fluorescence before reduction of CPP to 30 mm Hg. (**d**) Micrograph taken from the same area after reduction of CPP to 30 mm Hg by increasing ICP displays increased NADH fluorescence, showing a reduction in oxygen consumption and tissue hypoxia.

CPP	MAP group	ICP group
30	(2/10)	(8/10)
50	(0/10)	(3/10)
70	(0/10)	(0/10)

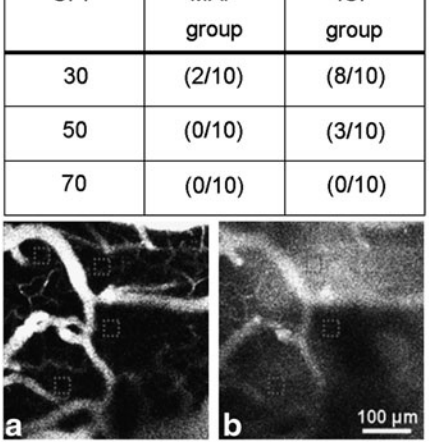

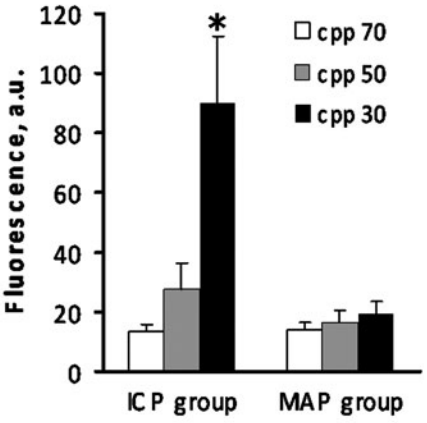

FIG. 3. Incidence of blood–brain barrier (BBB) permeability breakdown in rats subjected to reduced cerebral perfusion pressure (CPP) from 70, 50, and 30 mm Hg by decreasing mean arterial pressure (MAP) or increasing intracranial pressure (ICP) as demonstrated by increased fluorescein isothiocyanate-labeled dextran fluorescence. Shown are readings in the red squares on the micrographs at baseline CPP (**a**) and at CPP of 30 mm Hg (**b**) with extravasation of fluorescein dye into the tissue. The graph illustrates the mean ± standard error of the mean (SEM; $n = 10$ rats/group) of fluorescein isothiocyanate fluorescence in absolute units (a.u.) at CPP of 70, 50, and 30 mm Hg by increasing ICP and decreasing MAP.

by high ICP, whereas no significant differences were observed in the MAP group.

Brain water content

Changes in normalized cortical water content as percentage of controls at different CPP are shown in Figure 4 (mean ± SEM). In the high ICP group, significant increases in brain water content occurred at CPP of 50 ($p < 0.05$) and 30 mm Hg ($p < 0.01$) compared to controls. In the MAP group, significant changes in brain water content were not seen. It should be noted that the cortical water content obtained by *in vivo* scooping of the brain sample through the craniotomy averaged 72.9 ± 0.47% ($n = 10$), which was significantly lower than the value of 79.58 ± 0.76% ($n = 10$) obtained by decapitation, removal of the brain from the calvarium, and sampling the cortex for wet/dry weight determination of brain water content. The reasons for this discrepancy are discussed later.

Discussion

Our study showed that the apparent reduction in the critical CPP for CBF autoregulation from 60 to 30 mm Hg when CPP was reduced by increasing ICP as opposed to decreasing MAP is attributable to an increase in high-velocity flow through large-diameter microvessels, which we refer to as TFC shunts. The fact that this increase in high-velocity large-diameter (i.e., 8–15 μm) as opposed to smaller-diameter 3–7 μm capillaries was accompanied by the development of brain tissue hypoxia and edema, a hallmark of non-nutritive shunt flow, which strongly suggests a transition from CAP to TFC shunt flow. A simple increase in flow velocity through larger microvessels without shunting would not be consistent with tissue hypoxia and edema. Instead, it should result in improved tissue oxygenation.

We have demonstrated for the first time a definitive transition from low-velocity microvessel to high-velocity microvessel flow, induced by decreasing CPP by raising ICP, which

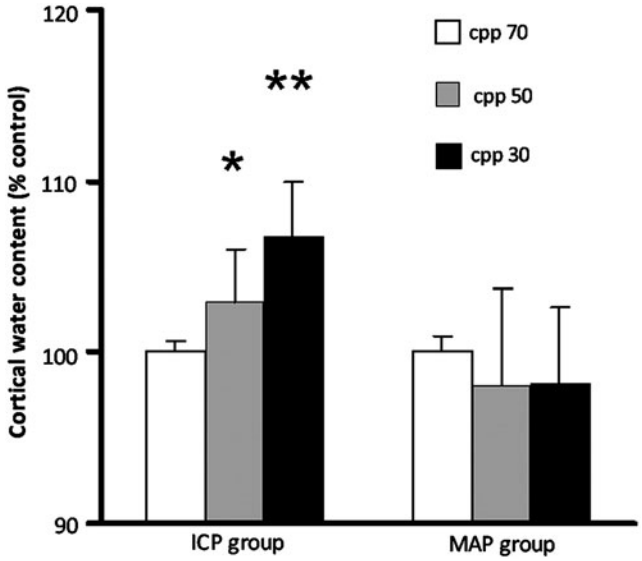

FIG. 4. Cortical water content in percentage of controls as measured by dry/wet weight in the rat parietal cortex at cerebral perfusion pressures (CPP) of 70, 50, and 30 mm Hg, by either intracranial pressure (ICP) increase (ICP group), or mean arterial pressure (MAP) reduction (MAP group). Decreasing CPP from 70 to 50 and 30 mm Hg by high ICP increased cortical water content significantly (*$p < 0.05$, **$p < 0.01$, respectively) ($n = 3$ rats for each CPP), compared to a normal CPP of 70 mm Hg ($n = 6$ rats). In the MAP group cortical water content was no different from controls ($n = 3$ rats for each CPP level). Data are presented as mean ± standard error of the mean (SEM). The control water content value at a CPP of 70 mm Hg was 72.9 ± 0.47% ($n = 10$) by scooping, which was significantly lower than the value of 79.58 ± 0.76% ($n = 5$) obtained by removal of the brain from the calvarium.

did not occur by reducing MAP. The significance of this observation is that we now have a method or probe that can be used to directly quantify the critical relationships and interaction between ICP and CPP, such as whether the detrimental effects of an ICP of 40 mm Hg induces a transition to TFC shunt flow can be delayed or prevented by increasing CPP.

The demonstration of a transition from capillary to what we call TFC shunt flow by increasing ICP to decrease CPP that did not occur when CPP was reduced by decreasing MAP positively identifies ICP as the essential component in this transition. It is not often appreciated that cerebral venous pressure (CVP) must exceed ICP if brain perfusion is to continue, as was shown in earlier studies (Nakagawa et al., 1974; Schulman and Verdier, 1967). While the increase in CVP with the increase in ICP may serve to keep cerebral veins open in the face of increased ICP (Pranevicius and Pranevicius, 2002), it occurs at the price of increasing both capillary pressure, which increases capillary wall stress, and BBB permeability (Mayhan and Heistad, 1986). The increase in CVP and thereby capillary hydrostatic pressure promotes the development of brain edema (Schulman and Verdier, 1967). Thus, as illustrated in Figure 5, with the rise in ICP, CVP increases, which reflects retrograde to increased capillary pressure, thereby inducing tissue edema, increased capillary resistance, and a transition to lower resistance, non-nutritive TFC shunts (Yada et al., 1973; Nemoto, 2006). TFC shunt flow leads to tissue hypoxia and edema, which further increases ICP in a positive feedback loop. Precisely at what ICP and CPP this transition occurs, and at what combination of ICP, CVP, and CPP, remain as objectives for future studies.

The complexity of the relationships between ICP, CVP, and CPP is partly a function of the heterogeneity of the cerebral vasculature, which increases in going from global, regional, and microvascular-neuronal with tight flow-metabolism coupling (Shinozuka et al., 1989; Thompson et al., 2004; Waschke et al., 2004). Heterogeneity in CBF is also seen in CBF autoregulation at the microvascular level, varying from no autoregulation to perfect autoregulation (Jones et al., 2002), suggesting that at the microvascular level, different brain regions normally exist in different stages of ischemic stress (Goldman, 2008; Schizler et al., 2003; Shinozuka et al., 1989; Thompson et al., 2004), which could also result in variable local susceptibility to tissue hypoxia (Tuunanen et al., 2006) and brain edema as well as CBF autoregulation. Using a 0.8-mm-diameter Doppler probe we did not observe perfect maintenance of CBF with a reduction of CPP from 70 to 50 mm Hg, where at least in the high ICP group perfect autoregulation would be expected. However, previous investigators have also reported less than perfect CBF autoregulation. There was about a 3% reduction in CBF for every 10% change in arterial pressure in rats using Doppler flux with a 1-mm-diameter probe (Dirnagl and Pulsinelli, 1990). In baboons, there was a progressive decrease in CBF as measured in regions of interest (ROI) 1.0 cm in diameter, with decreasing MAP from 120 to 60 mm Hg (Schumann et al., 1998). Thus, it is not unexpected that our studies using a 0.8-mm-diameter Doppler probe showed less than perfect autoregulation, which appears to be a function of the small volume of tissue sampled in the measurement of CBF, as previously shown (Jones et al., 2002). The important point is that there were differences in the changes in Doppler flux between the ICP and MAP groups, with Doppler flow higher in the former that could be a reflection of shunt flow.

Reduction of arterial pressure by phlebotomy likely resulted in a baroreceptor reflex via the aortic body pressure receptors (Stanfield and Germann, 2008). Likewise, the increase in ICP also resulted in a Cushing reflex (Fitch et al., 1977), with an increase in arterial pressure to maintain cerebral perfusion in the face of rising ICP. In both of these circumstances the rise in arterial pressure was prevented by graded phlebotomy in an effort to regulate CPP. These responses are both mediated via the sympatho-adrenal systems that increase plasma catecholamine (adrenalin and noradrenalin) levels. The effects of

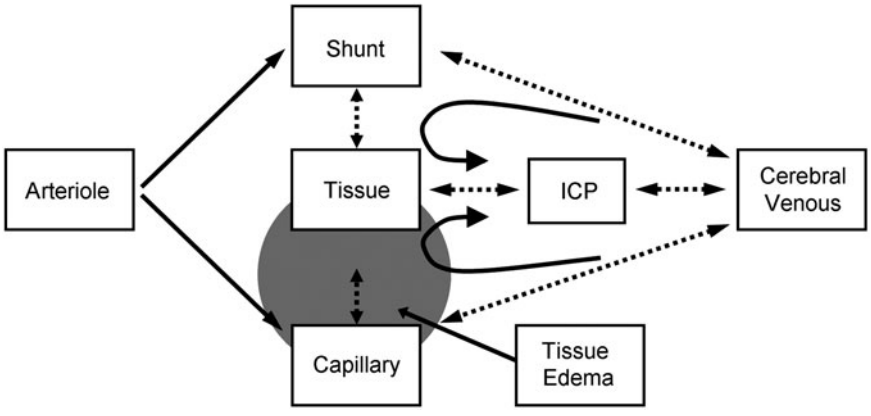

FIG. 5. Hypothesized mechanisms for what we surmise to be a transition from capillary to thoroughfare channel shunt flow as a result of increased intracranial pressure (ICP). Arteriole inflow on the left of the figure, normally goes primarily through capillaries, while an unknown but presumably small fraction goes through thoroughfare channel (TFC) shunts, due to the much lower resistance through the capillaries. When ICP increases, cerebral venous pressure increases, and must exceed ICP in order for perfusion to continue. The increased venous pressure transmits retrograde to the capillaries, resulting in the development of tissue edema and hypoxia, further exacerbating the increase in ICP and venous pressure in a positive feedback loop. Eventually, capillary resistance exceeds that of the TFC shunts, and the transition to TFC shunt flow begins. Dotted lines and double-ended arrows indicate reciprocal interactions. Circular arrows indicate hydrostatic pressure recoil of ICP through the cerebral venous system back to the capillaries, which contributes to tissue edema, raised ICP, and a further increase in cerebral venous and capillary pressures in a positive feedback loop.

circulating catecholamines on cerebral perfusion and metabolism are reportedly minimal (Horinaka et al., 1997), which may be due to enzyme barriers to calcium receptors such as catechol-O-methyl transferase (COMT) (McCalden et al., 1997, 1979). However, in circumstances in which the BBB may be breached through arterial hypertension, as in the breakthrough of CBF autoregulation and circulating catecholamines, may penetrate the BBB, thereby stimulating brain metabolism and increased CBF (Ekstrom-Jodal et al., 1975; Skinhoj, 1973). An increase in BBB permeability was not observed in the MAP group, but only in the ICP group, suggesting that circulating catecholamines may have stimulated brain metabolism and blood flow in the ICP group, exacerbating the development of edema and a transition to microvascular shunt flow. However, these factors remain to be elucidated in future studies.

A reduction in capillary density in ischemic and infracted brain has been demonstrated by positron emission tomography in stroke (Gjedde, 1991; Gjedde and Kuwabara, 1993), in edema (Tomita, 1968), and in sepsis (Ince and Sinaasappell, 1999; Taccone et al., 2010). These observations support the concept of brain microvascular shunting, since it is well established that severe hyperemia due to non-nutritive flow occurs in infarcted tissue, the same tissue in which capillary rarefaction occurs. The transition from CAP to TFC shunts is expected to increase the inter-microvascular distance, leading to tissue hypoxia due to the increase in diffusion distance for oxygen (Masamoto and Tanishita, 2009; Moppett and Hardman, 2007).

Consistent with the rarefaction of capillaries in infarcted brain and non-nutritive shunt flow is the increase in brain edema, which is believed to be due to an increase in back pressure from ICP to CVP to capillaries. The increase in brain water content was substantial, by about 5%, from 73% to 78%. While the magnitude of the increase in brain water content appears to be high, an increase in brain water content of 8% was reported in rats subjected to middle cerebral artery occlusion, for which brain water content increased from 78% to 86% over 2 days (Hatashita and Hoff, 1990). The increase in brain water content we report is due to an increase in ICP, and not simply ischemia, and may thereby result in more edema. The control rat brain water content of $72.9 \pm 0.47\%$ obtained by scooping the cortical tissue through the craniotomy at a CPP of 70 mm Hg was lower than the water content obtained by the conventional method of decapitation. Removal of the brain from the skull after decapitation and taking a tissue sample for brain water content by wet/dry weight resulted in a water content ranging between 78% and 79% (Chen et al., 2006; Nakamura et al., 2008; Wasserman and Schlichte, 2007), and in our hands $79.58 \pm 0.76\%$ ($n = 10$). However, the effect of rapid sampling on the measurement of brain tissue water content has not been previously compared. In our comparison, the higher value of $79.58 \pm 0.76\%$ we obtained by decapitation and removal of the brain attests to the accuracy of our measurements. One possibility for the lower water content is that the volume of tissue sampled was lower than that obtained after decapitation and removal of the brain from the calvarium, resulting in a greater evaporation error. The mean weight of tissue sampled by scooping of 56.8 ± 26.09 mg, compared to 77.4 ± 34.97 mg by brain removal, was lower, but the difference was not significant ($p > 0.05$). We believe that the difference in the two methods regarding brain water content has to do with the shift of extracellular fluid to the intracellular space, which begins within seconds to minutes after decapitation in chickens (Ruis-Heutinck et al., 1988), and after focal ischemia in cats (Matsuoka and Hossmann, 1982). This rapid shift of fluid from the extracellular to the intracellular space may account for the difference in cortical brain water content seen between the two methods. Nevertheless, using the scooping method, we showed a clear increase in brain water content with decreasing CPP induced by increased ICP, but not with decreasing MAP. Again, the development of tissue hypoxia and brain edema strongly suggests that the increase in high-velocity flow through larger-diameter microvessels was TFC non-nutritive shunt flow, rather than simply an increase in flow velocity through precapillary arterioles and venules that range from 8–15 μm in diameter.

Two aspects of this study have important implications for future studies on the relationship between ICP and CPP, and in the clinical management of patients suffering brain edema and high ICP. First, we now have identified a measurable variable (i.e. CAP:TFC shunt ratio), which can be used to study the detrimental or beneficial effects of various ICP-CPP interactions, and the potential beneficial effects of various therapeutic interventions in preventing the transition to shunt flow. For example, can the detrimental effects of high ICP on shunt flow be circumvented by increasing CPP above the clinically defined target of 60–70 mm Hg? Our preliminary data (unpublished) suggest that increasing CPP in the face of rising ICP raises the threshold for shunting.

Second, using this concept of the CAP:TFC ratio as a measure of shunting, we can now evaluate the efficacy of decreasing ICP pharmacologically, while maintaining a relatively low CPP of 60 mm Hg, as suggested by the "Lund concept" (Grande et al., 2002; Nordstrom, 2003). Does the pharmacological reduction of ICP have a greater impact on the resolution of brain edema and the vicious cycle of high ICP and CVP than an increase in CPP? These are very important, clinically-relevant questions that can now be addressed using the CAP:TFC ratio to define thresholds for ICP and CPP, and the efficacy of therapeutic interventions on shunting.

Finally, our studies were done on the normal brain rather than the traumatized or injured brain. The relationships between CPP and ICP defined by the CAP:TFC ratio in the injured brain we suspect could differ markedly from that in the normal brain. The injured brain with brain edema and high ICP would likely be highly sensitive to increases in CVP, whether due to a raised ICP or hyperemia. What these relationships are in the injured brain have yet to be defined.

In summary, the importance of our findings in this study is that we have shown that increased ICP induces a definitive transition from CAP to high-velocity, large-microvessel flow, which we believe to be TFC shunt flow, based on the associated development of tissue hypoxia and brain edema, hallmarks of nonnutritive shunt flow. Some of the important clinical questions pertaining to management of patients with high ICP can be studied objectively and quantitatively with this model using 2PLSM.

Acknowledgments

The two-photon facility was supported by the University of New Mexico (UNM) HSC COBRE program (P20 RR15636). This research was supported by NIH grants NS061216 and NS051639.

Author Disclosure Statement

No competing financial interests exist.

References

Abdul-Rahman, A., Dahlgren, N., Johansson, B.B., and Siesjö, .B.K. (1979). Increase in local cerebral blood flow induced by circulating adrenaline: involvement of blood-brain barrier dysfunction. Acta Physiol. Scand. 107, 227–232.

Barry, D.I., Strandgaard, S., Graham, D.I., Braendstrup, O., Svendsen, U.G., Vorstrup, S., Hemmingsen, R., and Bolwig, T.G. (1982). Cerebral blood flow in rats with renal and spontaneous hypertension: resetting of the lower limit of autoregulation. J. Cereb. Blood Flow Metab. 2, 347–353.

Chance, B., Cohen, P., Jobsis, F., and Schoener, B. (1962). Intracellular oxidation-reduction states in vivo. Science 137, 499–508.

Chen, C.H., Toung, T.J.K., Sapristein, A., and Bhardwaj, A. (2006). Effect of duration of osmotherapy on blood-brain barrier disruption and regional cerebral edema after experimental stroke. J. Cereb. Blood Flow Metab. 26, 951–958.

Dirnagl, U., and Pulsinelli, W. (1990). Autoregulation of cerebral blood flow in experimental focal cerebral ischemia. J. Cereb. Blood Flow Metab. 10, 327–336.

Ekstrom-Jodal, B., Haggendal, E., Johansson, B., Linder, L.-E., and Nilsson, N.J. (1975). Acute arterial hypertension and the blood brain barrier: An experimental study in dogs, in: *Cerebral Circulation and Metabolism*. T.W. Langfitt, L.C. McHenry, M. Reivich, and H. Wollman (eds). Springer Verlag: New York. pps. 7–9.

Feindel, W., and Perot, P. (1965). Red cerebral veins: A report on arteriovenous shunts in tumors and cerebral veins: A report on arteriovenous shunts in tumors and cerebral scars. J. Neurosurg. 22, 315–325.

Feindel, W., Yamamoto, Y.L., and Hodge, C.P. (1971). Red cerebral veins and the cerebral steal syndrome. Evidence from fluorescein angiography and microregional blood flow by radioisotopes during excision of an angioma. J. Neurosurg. 35, 167–179.

Fitch, W., McDowall, D.G., Keaney, N.P., and Pickerodt, V.W. (1977). Systemic vascular responses to increased intracranial pressure. The 'Cushing' response in the presence of intracranial space-occupying lesions: systemic and cerebral haemodynamic studies in the dog and the baboon. J. Neurol. Neurosurg. Psychiatry 40, 843–852.

Gjedde, A., and Kuwabara, H. (1993). Absent recruitment of capillaries in brain tissue recovering from stroke. Acta Neurochir. Suppl. 57, 35–40.

Gjedde, A. (1991). Pathophysiology of the human brain after stroke, monitored by positron emission tomography. Exp. Pathol. 42, 221–227.

Ginsberg, M.D., Dietrich W.D., and Busto, R. (1987). Couple forebrain increases of local cerebral glucose utilization and blood flow during physiologic stimulation of a somatosensory pathway in the rat: Demonstration by double-label autoradiography. Neurology 37, 11–19.

Grande, P.O., Asgiersson, B., and Nordstrom, C.H. (2002). Volume targeted therapy of increased intracranial pressure: the Lund concept unifies surgical and non-surgical treatments. Acta Anesthesiol. Scand. 46, 929–941.

Goldman, D. (2008). Theoretical models of microvascular oxygen transport to tissue. Microcirculation 15, 795–811.

Grubb, R.L. Jr., Raichle, M.E., Phelps, M.E., and Ratcheson, R.A. (1975). Effects of increased intracranial pressure on cerebral blood volume, blood flow, and oxygen utilization in monkeys. J. Neurosurg. 43, 385–398.

Haggendal, E., Nilsson, N.J., and Norback, B. (1965). On the components of Kr85 clearance curves from the brain of the dog. Acta Physiol. Scand. 258, 1–25.

Hasegawa, T., Ravens, J.R., and Toole, J.F. (1967). Precapillary arteriovenous anastomoses. "Thoroughfare channels" in the brain. Arch. Neurol. 16, 217–224.

Hatashita, S., and Hoff, J.T. (1990). Brain edema and cerebrovascular permeability during cerebral ischemia in rats. Stroke 21, 582–588.

Hauck, E.F., Apostel, S., Hoffmann, J.F., Heimann, A., and Kempski, O. (2004). Capillary flow and diameter changes during reperfusion after global cerebral ischemia by intravital video microscopy. J. Cereb. Blood Flow Metab. 24, 383–391.

Hauerberg, J., and Juhler, M. (1994). Cerebral blood flow autoregulation in acute intracranial hypertension. J. Cereb. Blood Flow Metab. 14, 519–525.

Horinaka, N., Artz, N., Cook, M., Holmes, C., Goldstein, D.S., Kennedy, C., and Sokoloff, L. (1997). Effects of elevated plasma epinephrine on glucose utilization and blood flow in conscious rat brain. Am. J. Physiol. 272, 1666–1671.

Hudetz, A.G., Wood, J.D., and Kampine, J.P. (2000). 7-Nitroindazole impedes erythrocyte flow response to isovolemic hemodilution in the cerebral capillary circulation. J. Cereb. Blood Flow Metab. 20, 220–224.

Hudetz, A.G., Biswal B., Geher G., and Kampine J.P. (1997a). Effects of hypoxia and hypercapnia on capillary flow velocity in the rat cerebral cortex. Microvasc. Res. 54, 35–42.

Hudetz, A.G. (1997). Blood flow in the cerebral capillary network: a review emphasizing observations with intravital microscopy. Microcirculation 4, 233–252.

Hudetz, A.G., Feher, G., and Kampine, J.P. (1996). Heterogeneous autoregulation of cerebrocortical capillary flow: evidence for functional thoroughfare channels? Microvasc. Res. 51, 131–136.

Hudetz, A.G., Fehér, G., Weigle, C.G., Knuese, D.E., and Kampine, J.P. (1995). Video microscopy of cerebrocortical capillary flow: response to hypotension and intracranial hypertension. Am. J. Physiol. 268, 2202–2210.

Hughes, R.L., Yonas, H., Gur, D., and Latchaw, R. (1989). Cerebral blood flow determination within the first 8 hours of cerebral infarction using stable xenon-enhanced computed tomography. Stroke 20, 754–760.

Ince, C., and Sinaasappell, M. (1999). Microcirculatory shunting in sepsis and shock. Crit. Care Med. 27, 1369–1377.

Ito, H., Iida, H., Kinoshita, T., Hatazawa, J., Shimosegawa, E., Okudera, T., and Kanno, I. (2000). Regional differences in cerebral vascular response to $PaCO_2$ changes in humans measured by positron emission tomography. J. Cereb. Blood Flow Metab. 20, 1264–1270.

Ingvar, D.H., and Lassen, N.A. (1977). Cerebral function, metabolism and blood flow. News and trends from the VIIIth international CBF symposium in Copenhagen.

Johnston, I.H., Rowan, J.O., Harper, A.M., and Jennett, W.B. (1972). Raised intracranial pressure and cerebral blood flow: Cisterna magna infusion in primates. J. Neurol. Neurosurg. Psychiatry 35, 285–296.

Jones, S.C., Radinsky, C.R., Furlan, A.J., Chyatte, D., Qy, Y., Easly, K., and Perez-Trepichio, A. (2002). Variability in the magnitude of the cerebral blood flow response and the shape of the cerebral blood flow: Pressure autoregulation curve during hypotension in normal rats. Anesthesiology 97, 488–496.

Kleinfeld, D., Mitra, P.P., Helmchen, F., and Denk, W. (1998). Fluctuations and stimulus-induced changes in blood flow

observed in individual capillaries in layers 2 through 4 of rat neocortex. Proc. Natl. Acad. Sci. USA 95, 15741–15746.

Lassen, N.A., and Perl, W. (1979). Compartmental analysis, in: *Tracer Kinetic Methods in Medical Physiology.* Raven Press: New York, pp. 137–155.

Mathew, N.T., Meyer, J.S., Hartmann, A., and Ott, E.O. (1975). Abnormal cerebrospinal fluid-blood flow dynamics. Implications in diagnosis, treatment, and prognosis in normal pressure hydrocephalus. Arch. Neurol. 32, 657–664.

Masamoto, K., and Tanishita, K. (2009). Oxygen transport in brain tissue. J. Biomech. Eng. 131, 074002-1-6.

Matsuoka, Y., and Hossmann, K.A. (1982). Cortical impedance and extracellular volume changes following middle cerebral artery occlusion in cats. J. Cereb. Blood Flow Metab. 2, 466–477.

Mayhan, W.G., and Heistad, D.D. (1986). Role of veins and cerebral venous pressure in disruption of the blood-brain barrier. Circulation Res. 59, 216–220.

McCalden, T.A., Eidelman, B.H., and Mendelow, A.D. (1997). Barrier and uptake mechanisms in the cerebrovascular response to noradrenaline. Am. J. Phsiol. 233, 458–465.

McCalden, T.A., Mendelow, A.D., Coull, A., Scriven, D.R., Rosendorff, C., and Eidelman, B.H. (1979). Role of catecholamine degradative enzymes and the adrenergic innervation in determining the cerebrovascular response to infused norepinephrine. Stroke 10, 319–322.

Miller, J.D., Stanek, A., and Langfitt, T.W. (1972). Concepts of cerebral perfusion pressure and vascular compression during intracranial hypertension. Prog. Brain. Res. 35, 411–432.

Moppett, I.K., and Hardman, J.G. (2007). Modeling the causes of variation in brain oxygen. Anesth. Anesth. Analg. 105, 1104–1112.

Motti, E.D., Imhof, H.G., and Yasargil, M.G. (1986). The terminal vascular bed in the superficial cortex of the rat. An SEM study of corrosion casts. J. Neurosurg. 65, 834–846.

Nakagawa, Y., Tsuru, M., and Yada, K. (1974). Site and mechanism for compression of the venous system during experimental intracranial hypertension. J. Neurosurg. 41, 427–434.

Nakamura, T., Kuroda, Y., Yamashita, S., Zhang, X., Miyamoto, O., Tamiya, T., Nagao, S., Xi, G., Keep, R.F., and Itano, T. (2008). Edavarone attenuates brain edema and neurologic deficits in a rat model of acute intracerebral hemorrhage. Stroke 39, 463–469.

Nemoto, E.M. (2006). Dynamics of cerebral venous and intracranial pressures. Acta Neurochir. Suppl. 96, 435–437.

Nordstrom, C.H. (2003). Assessment of critical thresholds for cerebral perfusion pressure by performing bedside monitoring of cerebral energy metabolism. Neurosurg. Focus 15, 1–8.

Pranevicius, M., and Pranevicius, O. (2002). Cerebral venous steal: Blood flow diversion with increased tissue pressure. Neurosurgery 51, 1267–1274.

Ravens, J.R. (1974). Anastomoses in the vascular bed of the human cerebrum, in: *Pathology of Cerebral Microcirculation*. J. Cervos-Navaro (ed). Walter de Gruyter: Berlin, pps. 26–38.

Rosner, M.J., Rosner, S.D., and Johnson, A.H. (1995). Cerebral perfusion pressure management protocol and clinical results. J. Neurosurg. 83, 949–962.

Ruis-Heutinck, L.F.M., Savenije, B., Postema, F., Van Voorst, A., Lambooij, E., and Korf, J. (1988). Impedance recordings to determine change in extracellular volume in the brain following cardiac arrest in broiler chickens. Poultry Sci. 77, 1422–1427.

Schizler, I., Tomita, M., Fukuuichi, Y., Tanahashi, N., and Inoue, K. (2003). New optical method for analyzing cortical blood flow heterogeneity in animals: validation of the method. Am. J. Physiol. Heart. Circ. Physiol. 279, 1291–1298.

Schulman, K., and Verdier, G.R. (1967). Cerebral vascular resistance changes in response to cerebrospinal fluid pressure. Am. J. Physiol. 213, 1084–1088.

Schumann, P., Touzani, O., Young, A.R., Baron, J.C., Morello, R., and MacKenzie, E.T. (1998). Brain 121, 1369–1379.

Seylaz, J., Charbonné, R., Nanri, K., Von Euw, D., Borredon, J., Kacem, K., Méric, P., and Pinard, E. (1999). Dynamic in vivo measurement of erythrocyte velocity and flow in capillaries and of microvessel diameter in the rat brain by confocal laser microscopy. J. Cereb. Blood Flow Metab. 19, 863–870.

Shinozuka, T., Nemoto, E.M., and Winter, P.M. (1989). Mechanisms of cerebrovascular O_2 sensitivity from hyperoxia to moderate hypoxia in the rat. J. Cereb. Blood Flow Metab. 9, 187–195.

Skinhoj, E. (1973). Hemodynamic studies within the brain during migraine. Arch. Neurol. 29, 95–98.

Stanfield, C.L., and Germann, W.J. (2008). Principles of Human Physiology, 3rd ed. Pearson Benjamin Cummings: San Francisco.

Takano, T., Tian, G.F., Peng, W., Lou, N., Lovatt, D., Hansen, A.J., Kasischke, K.A., and Nedergaard, M. (2007). Cortical spreading depression causes and coincides with tissue hypoxia. Nat. Neurosci.10, 754–762.

Taccone, F.S., Su, F., Pierrakos, C., He, X., James, S., Dewitte, O., Vincent, J.L., and De Backer, D. (2010). Cerebral microcirculation is impaired during sepsis: an experimental study. Crit. Care. 14, 140.

Thompson, J.K., Peterson, M.R., and Freeman, R.D. (2004). High-resolution neurometabolic coupling revealed by focal activation of visual neurons. Nat. Neurosci. 7, 919–920.

Tomita, M. (1968). Significance of cerebral blood volume, in: *Cerebral Hyperemia and Ischemia: From the Standpoint of Cerebral Blood Volume.* M. Tomita, T. Sawada, H. Naritomi, and W.D. Heiss (eds). Excerpta Medica: Amsterdam, pps. 3–31.

Tuunanen, P.I., Murray, I.J., Parry, N.R.A., and Kauppinen, R.A. (2006). Heterogenous oxygen extraction in the visual cortex during activation in mild hypoxic hypoxia revealed by functional magnetic resonance imaging. J. Cereb. Blood Flow Metab. 26, 263–273.

Waschke, K.F., Riedel, M., Lenz, C., Albrect, D.M., von Ackern, K., and Kuschinsky, W. (2004). Regional heterogeneity of cerebral blood flow response to graded pressure-controlled hemorrhage. J. Trauma 56, 591–603.

Wasserman, J.K., and Schlichte, L.C. (2007). Minocycline protects the blood-brain barrier and reduces edema following intracerebral hemorrhage in the rat. Exp. Neurol. 207, 227–237.

Yada, K., Nakagawa, Y., and Tsuru, M. (1973). Circulatory disturbance of the venous system during experimental intracranial hypertension. J. Neurosurg. 39, 723–729.

Address correspondence to:
Denis E. Bragin, Ph.D.
University of New Mexico
Department of Neurosurgery
Domenici Hall/BRaIN Center
1101 Yale Boulevard NE
Albuquerque, NM 87131

E-mail: dbragin@salud.unm.edu